Automatic Segmentation of Aortic and Mitral Valves for Heart Surgical Planning of Hypertrophic Obstructive Cardiomyopathy

Limin Zheng   2100453062@email.szu.edu.cn
Hongyu Chen   2110456111@email.szu.edu.cn
Bo Meng   bomeng@szu.edu.cn
Shenzhen University

Qing Lu   qinglu0330@gmail.com
Jian Zhuang   zhuangjian5413@163.com
Xiaowei Xu   xiao.wei.xu@foxmail.com
Guangdong Provincial People's Hospital

Editors: Berrin Yanıkoğlu and Wray Buntine

Abstract

Hypertrophic obstructive cardiomyopathy (HOCM) is a leading cause of sudden cardiac death in young people. Septal myectomy surgery has been recognized as the gold standard for non-pharmacological therapy of HOCM, in which aortic and mitral valves are critical regions for surgical planning. Currently, manual segmentation of aortic and mitral valves is widely performed in clinical practice to construct 3D models used for HOCM surgical planning. Such a process, however, is time-consuming and costly. In this paper, we integrate anatomical prior knowledge into deep learning for automatic segmentation of aortic and mitral valves. In particular, a two-stage method is proposed: we first obtain the region of interest (RoI) from a CT image, where heart segmentation is then performed. The spatial relationship between heart substructures is utilized to identify a valve region that contains the aortic and mitral valves. Unlike typical two-stage methods, we feed the refined segmentation of the left ventricle, left atrium, and aorta as additional input for the valve segmentation. By incorporating this anatomical prior knowledge, deep neural networks (DNNs) can leverage the surrounding anatomical structures to improve valve segmentation. We collected a dataset of 27 CT images from patients with a medical history of septal myectomy surgery. Experimental results show that our method achieves an average Dice score of 71.2% and an improvement of 4.2% over existing methods. Our dataset and code will be released to the public Dataset.

Keywords: Hypertrophic obstructive cardiomyopathy, Surgical planning, Segmentation, Deep neural networks.

1. Introduction

Hypertrophic obstructive cardiomyopathy (HOCM) is a leading cause of sudden cardiac death in young people Maron and Maron (2013). Septal myectomy surgery is the mainstay of treatment for relief of left ventricular outflow tract obstruction (LVOT). It is effective in improving patient survival by removing a small amount of the thickened septal wall. The surgical treatment always comes with the repair of the mitral valve (MV) and the risk of

functional injury to the aortic valve (AV) for the reason that HOCM is often associated with structural abnormalities of MV Afanasyev et al. (2019).

To avoid the recurrence of the patient's disease after surgery, septal myectomy surgery requires extensive experience for surgeons, while the thickness and extent of hypertrophic myocardial resection are not easy to precisely grasp. Preoperative planning is essential for the surgeon to complete the procedure more smoothly, with the MV and AV being key areas for pathway planning. In routine operations, surgeons often lack spatial awareness of the travel a nd position of surgical tools during the process. To address this challenge, three dimensions (3D) printing can visualize the desired patients' cardiac structure in 3D to assist the surgeon in developing an individualized surgical strategy for the patient. Recently, manual 3D segmentation of valves, in addition to the large cardiac structures Xu et al. (2020)Xu et al. (2019), has been used in clinical applications Ma et al. (2021) for preoperative surgical planning. It can successfully assist surgeons in determining the location and anatomical characteristics of the target to personalize the patient's surgical strategy. However, manual segmentation is time-consuming, costly, and laborious Xu et al. (2018)Xu et al. (2023).

Recently, a variety of deep learning-based methods have been proposed for heart segmentation. In the light of the MICCAI'17 MM-WHS Zhuang and Shen (2016) challenge, various state-of-the-art heart segmentation models have been proposed and are summarised in Zhuang et al. (2019). For instance, Yang et al. (2017) proposed a modified 3D U-Net with a hybrid loss to alleviate the potential imbalance among different cardiac sub-structures to improve the whole heart segmentation performance. Meanwhile, some two-stage methods attract more and more attention in cardiac image analysis. Wang Chengjia et al. (2018) introduced a two-stage modified U-Net architecture, which simultaneously detected a region of interest (RoI) from the full volume and segmented the RoI at the original resolution. Payer et al. (2017) employed two CNNs in an end-to-end manner including location CNN and segmentation CNN for the whole heart segmentation. Although these methods achieve promising performance in large cardiac sub-structure, valves, especially AV and MV, have not been considered and explored.

Currently, there are a few methods related to valves segmentation in non-contrast CT images. Jin and Hugo (2021) applied Mask R-CNN and a combination of ResNet and U-Net respectively to segment chambers and valves, while Finnegan (2020) adopted a traditional machine learning method, multi-atlas mapping, for efficient segmentation. However, the performance is still limited, and a possible reason is that they do not take into account the domain knowledge to assist segmentation. Note that for preoperative surgical planning, AV and MV segmentation is quite an interesting problem. First, the target is rather small compared to the CT image as discussed in the background section. Second, based on our manual segmentation experience Ma et al. (2021) in clinical practice, extensive attention needs to be paid to the surrounding anatomies including the left ventricle (LV), the left atrium (LA), and the aorta (AO). Their relative positions help the detailed operation in the surgery. Such anatomical prior knowledge may help the segmentation of AV and MV.

In this paper, we propose a method that combines anatomical prior knowledge with deep learning techniques for the automatic segmentation of AV and MV. Our approach is based on a two-stage process: first, we extract the RoI from the CT image, followed by a refined segmentation step. A notable feature of our method is the inclusion of the refined
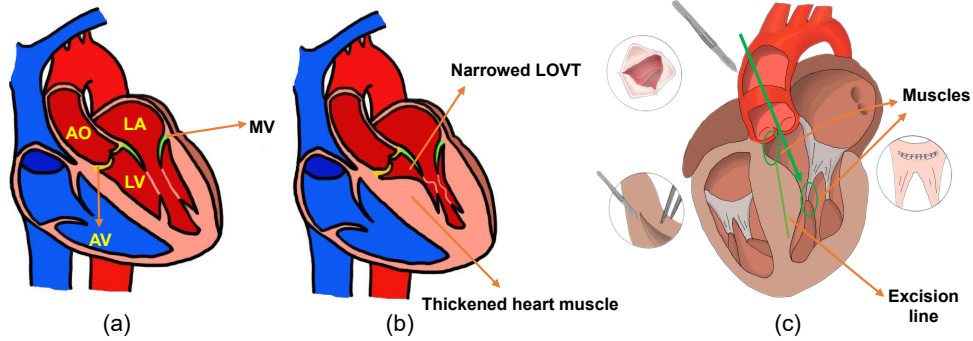
Figure 1: Background of HOCM including (a) normal heart structure, (b) heart structure of HOCM patients, and (c) the process of septal myectomy surgery. Note that the septal myocardium of HOCM patients is significantly thickened and their intraventricular chambers become smaller. As a result, LVOT becomes narrowed, leading to obstruction of blood in the heart. During the surgery, surgeons observe anatomic structures and operate in (c) along the green arrow line, and the relative positions between the myocardium and AV and MV play an important role in the surgery operation.

segmentation of the left ventricle, the left atrium, and the aorta as additional input for valve segmentation. This unique approach allows us to leverage the anatomical context provided by these surrounding structures during the deep neural network (DNN) training process. By incorporating this anatomical prior knowledge, we anticipate that the accuracy of the final valve segmentation can be improved. We collected the first dataset of 27 CT images from patients with a medical history of septal myectomy surgery. The experimental results show that our method achieves an average Dice score of 71.2%, representing a 4.2% improvement over existing methods in terms of segmentation accuracy. Our dataset and code will be released to the public Dataset.

2. Background

Anatomy: Normal cardiac anatomy is shown in Figure 1(a), showcasing a typical structure and function of the heart. However, in Figure 1(b), we observe HOCM, which is characterized by a significantly thickened ventricular wall. In HOCM, the anterior mitral valve leaflet exhibits anterior systolic motion. The thickened portion of the heart muscle in HOCM leads to a narrowed LVOT. This obstruction impedes the smooth flow of blood out of the left ventricle, posing a substantial risk of sudden cardiac death for affected patients. The obstruction of the LVOT is a prominent symptom of this disease, referred to as left ventricular outflow tract obstruction.

Septal myectomy surgery: In the clinical setting, patients usually require surgical intervention, specifically septal myectomy. This invasive surgical procedure involves the direct removal of a portion of the hypertrophied heart muscle. As shown in Figure 1(c), the surgeon needs to make an incision in the AO to access LV through AV for myocardial excision.
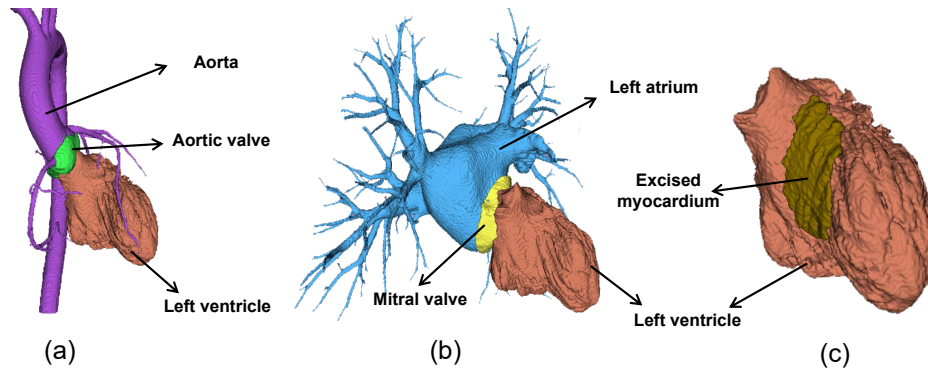
Figure 2: Illustration of the anatomy relationship among AO, LA, LV, valves, and the excision region. (a) 3D view of the anatomy relationship between AO, LV, and AV, (b) 3D view of the anatomy relationship between LA, LV, and MV, and (c) 3D view of the anatomy relationship between LV, and excised myocardium.

Additionally, if necessary, MV repair may also be performed. Additionally, if necessary, MV repair may also be performed. To ensure optimal surgical outcomes and minimize risks, preoperative evaluation of MV pathology is crucial. This evaluation helps determine whether additional MV repair is required in conjunction with the septal myectomy surgery. Furthermore, planning the surgical path based on the position of the AV is essential to reduce the risk of abnormal AV function. By assessing MV pathology and planning the surgical path according to the AV position, surgeons can enhance the effectiveness of procedures and minimize complications. This comprehensive approach allows for a smoother surgical process and helps optimize patient outcomes.

Relationships between substructures: Due to the limited contrast of the valve with its surrounding structures in CT images, the annotation of the valve is dependent on its anatomical relationship with other relevant structures. As shown in Figure 2, AV is located between AO and LV, while MV is located at the junction of LA and LV. Additionally, the myocardium that needs to be excised during the procedure is located on the ventricular wall within the LV. Considering these anatomical relationships, we regard the AO, LA, and LV as critical prior knowledge in the segmentation of the valves.

3. Dataset

Our dataset consists of 27 3D CT images captured by a Siemens SOMATOM Definition Flash machine. The ages of the associated patients range from 38 to 76 years with an average of 57.6 years. The size of the images is $512 \times 512 \times (275-571)$, and the typical voxel size is $0.25 \times 0.25 \times 0.5 mm^3$. The annotations were performed by two experienced radiologists, and the time for labeling each image is 0.5-1.5 hours. The labels include seven substructures: AV, MV, AO, LA, LV, myocardium, and excised myocardium. Figure 3 shows examples including CT images and their annotations in our dataset.

This work and the collection of data of retrospective data on implied consent received Research Ethics Committee (REC) approval from Guangdong Provincial People's Hospital
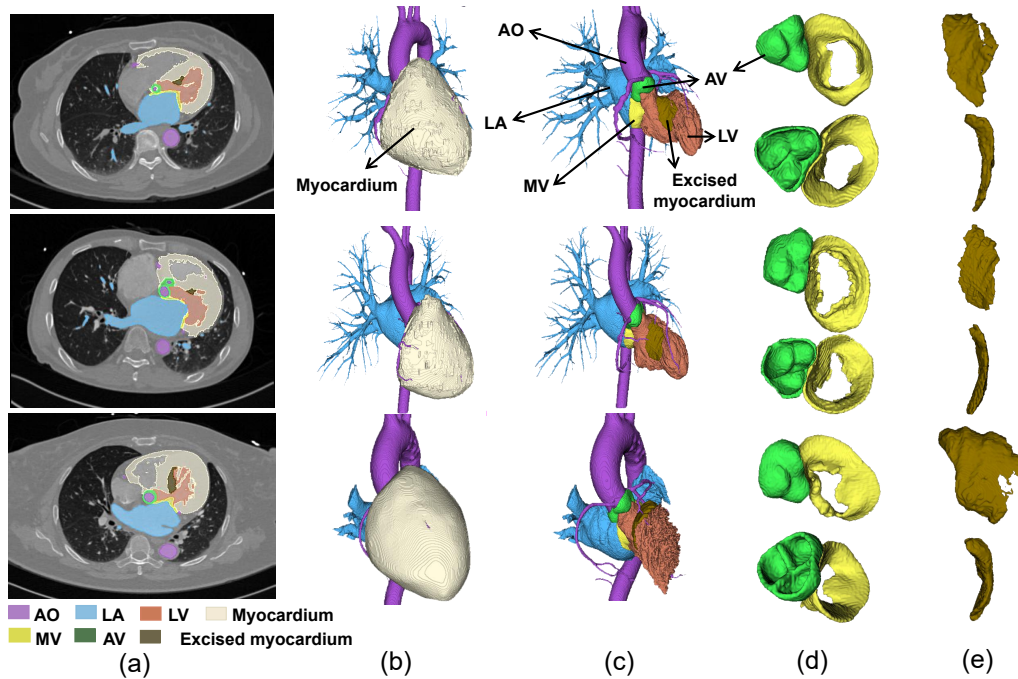
Figure 3: Illustration of the annotations in our dataset. including (a) 2D CT slices with corresponding labels, (b) 3D external views of the label, (c) 3D internal views of the label, (d) 3D views of combination of MV and AV in two viewpoints, and (e) 3D views of excised myocardium in two viewpoints.

under Protocol No. KY-N-2022-048-01. It complies with all relevant ethical regulations. Identification was performed in which all CT files are transformed into NIfTI format, and sensitive information including name, birth day, admission year, admission number, and CT number is removed. Only de-identified retrospective data were used for research, without active involvement of patients.

4. Method

4.1. Overview

The proposed method is illustrated in Figure 4, consisting of two main stages: the coarse stage and the refined stage. Like general two-stage methods Wang Chengjia et al. (2018), the coarse stage performed segmentation, which operates at a lower resolution, focuses on obtaining relevant information, such as the RoI. This initial segmentation step provides a coarse representation of the structures of interest. Moving on to the refined stage, the segmentation process operates at a higher resolution to achieve more detailed and accurate results. This stage refines the segmentation by incorporating additional contextual information. Unlike general two-stage methods, We specifically extract the valve region, which includes the junction between LV, LA, and AO, where the heart valves are situated. We
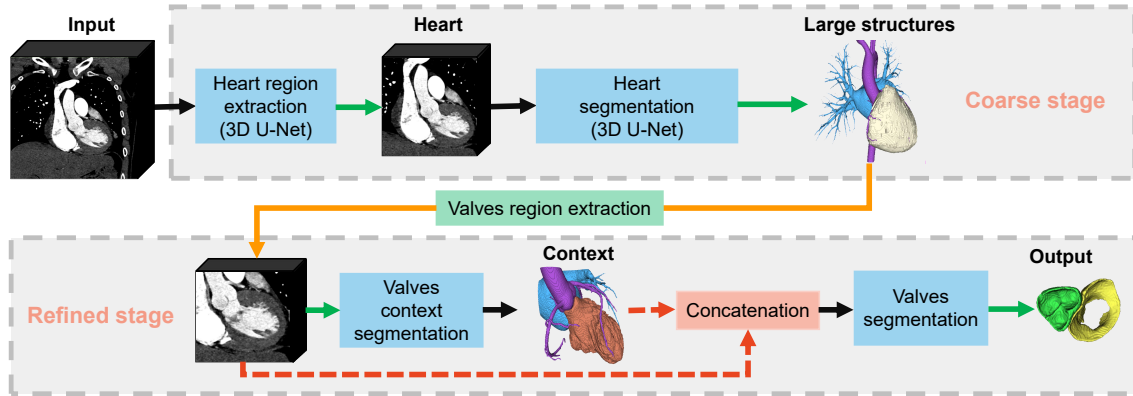
Figure 4: Overview of the proposed method combining CT image and valves context information (anatomical prior knowledge) as input for valves segmentation.

added a valves context segmentation module in the refined stage to obtain detailed segmentation of LV, LA, and AO which is subsequently utilized as extra information or anatomical prior knowledge for the valves segmentation task.

4.2. Heart region extraction

This step extracts the region that contains the heart and its connected vascular trunk. By doing so, unrelated areas can be eliminated, resulting in reduced redundant calculations and improved efficiency. Furthermore, this step contributes to accelerating the convergence of the model during the refined stage. Particularly, the CT images are resized to $128 \times 128 \times 128$ and subsequently fed to a 3D U-Net for segmentation of LA, LV, and AO. Following the segmentation, some simple post-processing techniques, such as erosion and the removal of small isolated islands, are applied. The combination of the LA, LV, and AO segmentations is then utilized to locate the RoI.

4.3. Heart segmentation

In this step, we aim to obtain the large heart substructures that are crucial for preoperative planning. These structures serve as the basis for extracting the spatial location of critical areas required for valve segmentation. Additionally, we make an effort to perform surgical resection site segmentation, although this task is subjective and relies heavily on the surgeon's experience. To achieve this, we utilize a 3D U-Net to segment several key structures in high resolution, including the AO, LA, LV, myocardium and excised myocardium. Since the size of RoI extracted from different patients varies, we normalize the RoI and divide it into a number of patches with a size of $128 \times 128 \times 128$ in a sliding window manner. In this way, we can obtain the context segmentation of large structures in the same resolution as the input image. By leveraging the anatomical spatial relationship between the AO, LA, and LV, we can then determine the valve region required for the refined stage of segmenta-

tion. This utilization of anatomical relationships helps ensure that the valve segmentation is performed accurately and effectively.

4.4. Valves region extraction

We use distance maps to crop the region of interest between AO, LA, and LV on CT images of the heart region as the valve region. The distance map is constructed as follows. First, euclidean distance is calculated between each pixel and target pixels belonging to AO, LV or LA, and the shortest distance is assigned. As a result, each pixel obtains three values corresponding to the shortest distance to AO, LV or LA, respectively. Then, a simple rule is used to crop the data. Particularly, pixels with a distance of [0, 60] to the AO and LV, and [0, 30] to LA are included. This distance effectively encompasses the aortic root and the junction of the LA and LV, which are the locations of AV and MV, respectively. The cropping of valve region and the 3D display of its annotation are shown in Figure 5. This visualization showcases the extracted valve region and its corresponding annotations, highlighting the effectiveness of the proposed method in accurately delineating the valve region of interest.

4.5. Valves context segmentation

The valves exhibit a distinct relationship with the surrounding structures, including the AO, LV, and LA as shown in Figure 6 in which the results of the heart segmentation module are presented with the ground truth of AV and MV. We can see that in the valve region, the AV part is roughly between AO and LV, and the MV part is between LA and LV. Though there exist intensive segmentation errors in the boundaries, the information on positions of related anatomic structures, i.e., valve context, can help localize the position of AV and MV. The valves region is divided into multiple patches with a size of 128×128×128 in a sliding window manner and then put into U-Net for segmentation. By employing this approach, we aim to enhance the accuracy and precision of the valve segmentation results, taking into account the contextual information provided by the neighboring structures.

4.6. Valves segmentation

The valves region and the segmentation of AO, LA, and LV from the context segmentation module are combined first and then divided into multiple patches with a size of 128×128×128 in a sliding window manner. In this way, two benefits are obtained. First, the resolution of the patches can be as high as the input CT image, and the sliding window can be regarded as some kind of ensemble to improve the segmentation performance. Second, a sliding window on a large RoI including AO, LV, and LA can extract a number of patches to ensure that AV and MV are included in the input.

5. Experiments

5.1. Experiment Setup

In the coarse stage, we use 3D U-Net to implement heart region extraction and large structures segmentation. To evaluate the effectiveness of incorporating anatomical prior knowl-
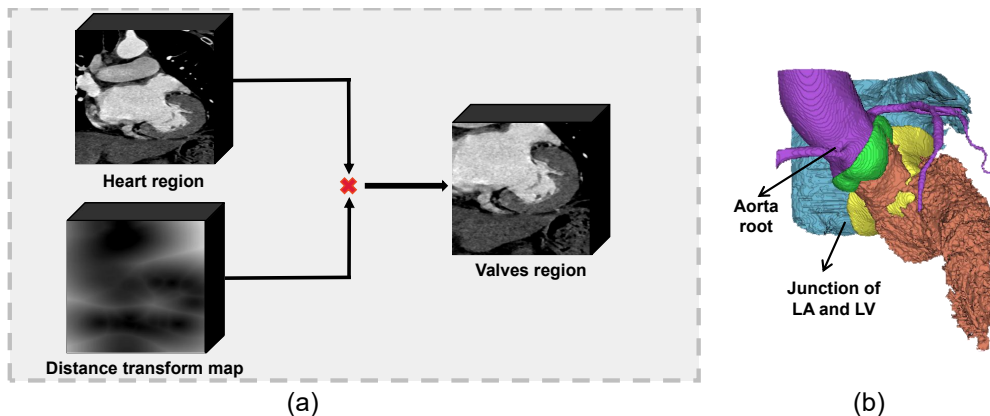
Figure 5: Details of valves context segmentation including (a) cropping of valve region using distance transform maps and (b) visualization of valve region annotations.
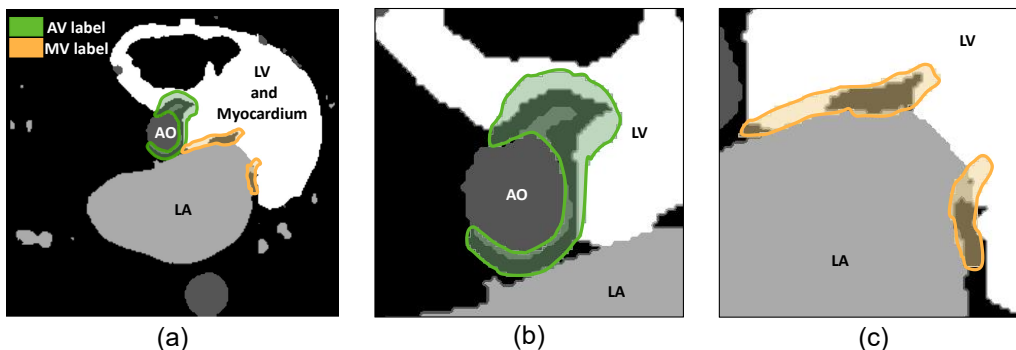

Figure 6: Illustration of valves context information. (a) The segmentation results of the heart segmentation module and its details for (b) AV and (c) MV show a close relationship between valves and surrounding anatomic structures.

edge in the refined stage, we conduct experiments using different types of inputs in various U-Net models. Additionally, in the refined stage, we aim to segment structures of different sizes together, which differs from the step-wise segmentation approach proposed in our method. All experiments were run on Nvidia A40 GPU with 48GB memory. As the data size is limited, three-fold cross-validation is adopted. The dataset is divided equally into three parts, two of which are used for training set and the remaining one for testing set. In the training set we randomly select two CT images as the validation set, and its Dice coefficient similarity(DSC) is used to adjust the learning rate. We set 0.003 as the initial learning rate and then adopt an adaptive adjustment strategy to modify the learning rate. DSC is used for evaluation. Both dice loss and focal loss are utilized in the training process, with 60 epochs for RoI segmentation and 40 epochs for valves segmentation. The window level

and window width are adjusted for contrast adjustment, and the min-max normalization method was used for data normalization.

5.2. Evaluation metrics

Dice similarity coefficient (DSC): DSC is commonly used to measure the effectiveness of medical image segmentation tasks, and it is an ensemble similarity metric that is usually used to calculate the similarity of two samples with a value threshold of [0, 1]. We used it to assess the agreement between the result of automatic segmentation and the manual labeling by the radiologist. DSC is defined as:

$$DSC = 2\frac{|A| \cap |B|}{|A| + |B|}, \tag{1}$$

where A is the result of automatic segmentation and B is the manual labeling by the radiologist.

True Positive Rate(TPR): True positive rate, also known as sensitivity, can reflect the extent to which the target structure is completely segmented with a value threshold of [0, 1]. TPR is defined as:

$$TPR = \frac{TP}{TP + FN}, \tag{2}$$

where TP is the correctly identified part of the automatic segmentation, and (TP+FN) is the ground truth.

Precision: Precision reflects the degree to which the target structure is correctly segmented with a value threshold of [0, 1]. Precision is defined as:

$$Precision = \frac{TP}{TP + FP}, \tag{3}$$

where (TP+FP) is the automatic segmentation.

Surface overlap (SO): The Surface Overlap (SO) metric is commonly used to evaluate the coverage or agreement between the segmentation results of a thin film-like structure and ground truth, with a value threshold of [0, 1]. It measures the overlapping region between the two segmentations. The metric considers a tolerable error distance, usually set to a certain value such as 1 mm, to account for small discrepancies in the thickness or position of the segmented valve. The surface within this tolerable error distance is considered as the overlapping part, indicating regions where the segmented valve and the reference segmentation agree. By using the SO metric, we can assess the accuracy and agreement of the valve segmentation results, taking into account the thin and complex structure of the valve. A higher SO value indicates better coverage and agreement between the segmentation results and the reference segmentation, while a lower SO value suggests discrepancies or errors in the segmentation.

Hausdorff Distance95 (HD95): We used the Hausdorff distance to assess the maximum mismatch between segmentation and manual annotation, which reflects the accuracy of the boundary. To calculate HD95, we ranked the distances between corresponding points on the segmented boundary and the manual annotation in descending order. Then, we identified the distance at the 5% of the ranked list, which represents the maximum mismatch tolerated for 95% of the boundary points.

Table 1: Mean and standard deviation (std) of DSC (in %) among various networks in different methods for AV and MV segmentation. Method A: Two-stage methods Wang Chengjia et al. (2018) in which five cardiac structures, (LA, LV, AO, MV, AV) are segmented simultaneously in the valve region. Method B: one-stage method Yang et al. (2017) in which MV and AV are segmented directly.

Backbones	Method	AV	MV	LV	LA	AO
Attention 3D U-Net	Our proposed	**72.1±9.7**	**70.2±6.0**	94.7±2.1	96.5±1.6	93.4±3.6
	Method A	67.3±14.2	68.5±8.8	94.5±2.5	96.3±1.7	93.0±3.9
	Method B	65.9±14.2	68.5±8.3	-	-	-
3D U-Net	Our proposed	**71.2±8.6**	**69.7±6.0**	92.1±8.5	95.8±2.6	92.9±3.6
	Method A	69.2±8.4	68.8±7.2	91.8±7.8	95.8±1.9	92.7±4.6
	Method B	68.3±9.7	66.3±13.9	-	-	-

Table 2: Mean and standard deviation (std) of DSC (in %) of the results in the heart segmentation module.

AO	LA	LV	Myocardium	Excised myocardium
89.8±7.1	91.7±3.1	92.1±3.3	87.0±3.9	62.9±11.3

Mean Surface Distance (MSD): For the valves, we also calculated the average surface distance between the segmentation results of the valves and the ground truth, reflecting the difference in thickness between them. This metric can provide the accuracy of reproducing the true thickness of the valves and be used to evaluate the performance in capturing the variations in thickness.

5.3. Quantitative result

The quantitative results of valves segmentation are shown in Table 1. Two backbones are also used for analysis. We can find that our method achieves the optimal DSC in the two backbones. Method A obtains a higher performance than Method B which is expected as Method A adopts two-stage methods which can better localize the region of interest than Method B. For the backbone using attention 3D U-Net, our method showed a 4.8% and 1.7% improvement in DSC in AV and MV, respectively, compared with Method A. While the backbone using 3D U-Net, our method showed a 2.0% and 0.9% improvement in DSC in AV and MV, respectively, compared with Method A. Thus, the average improvements achieved by our method over two-stage methods Wang Chengjia et al. (2018) are 3.4% and 1.3% for AV and MV, respectively.

The quantitative segmentation result of the heart segmentation module is shown in Table 2. For LV, LA, and AO, the average DSC can reach above 90%, which is quite high for preoperative spatial path planning. DSC for the excised myocardium is much lower than others which is because excised myocardium is largely subjective to the surgeons. Considering there are three surgeons for labeling for our dataset and there is no guidance in

clinical practice for precise segmentation of the excision region currently, high segmentation performance is relatively more challenging to achieve.
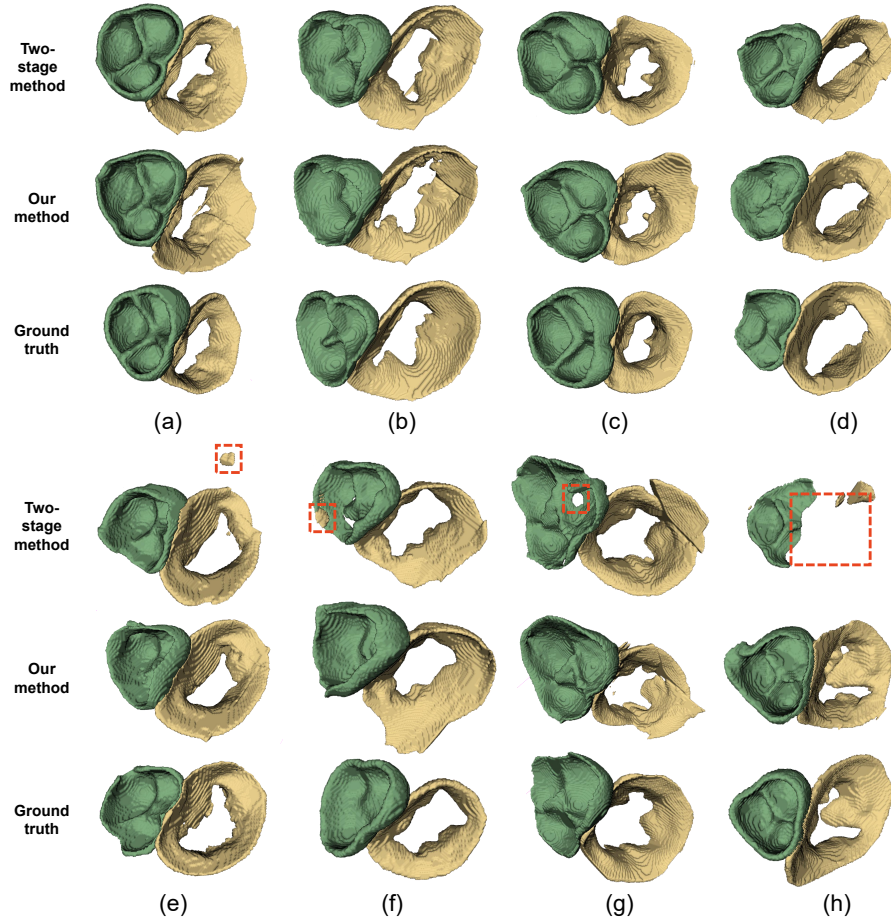

Figure 7: Visualization comparison of MV and AV segmentation by our method and the two-stage method Wang Chengjia et al. (2018).

5.4. Qualitative result

Qualitative comparison of MV and AV segmentation between our proposed method and the two-stage method Wang Chengjia et al. (2018) is shown in Figure 7. For many cases, both our method and the two-stage method can segment the valves quite well compared to the two-stage method as shown in Figure 7(a-d). However, we can also notice that there are some missing parts in the segmentation results of the two-stage method as shown in Figure 7(e-h), which is relatively hard to recognize. While our method can tackle the errors well especially for the case in Figure 7(h).

Qualitative illustration of the good and bad MV and AV segmentation by our method is shown in Figure 8. For good segmentation in Figure 8(a) and (e), median segmentation
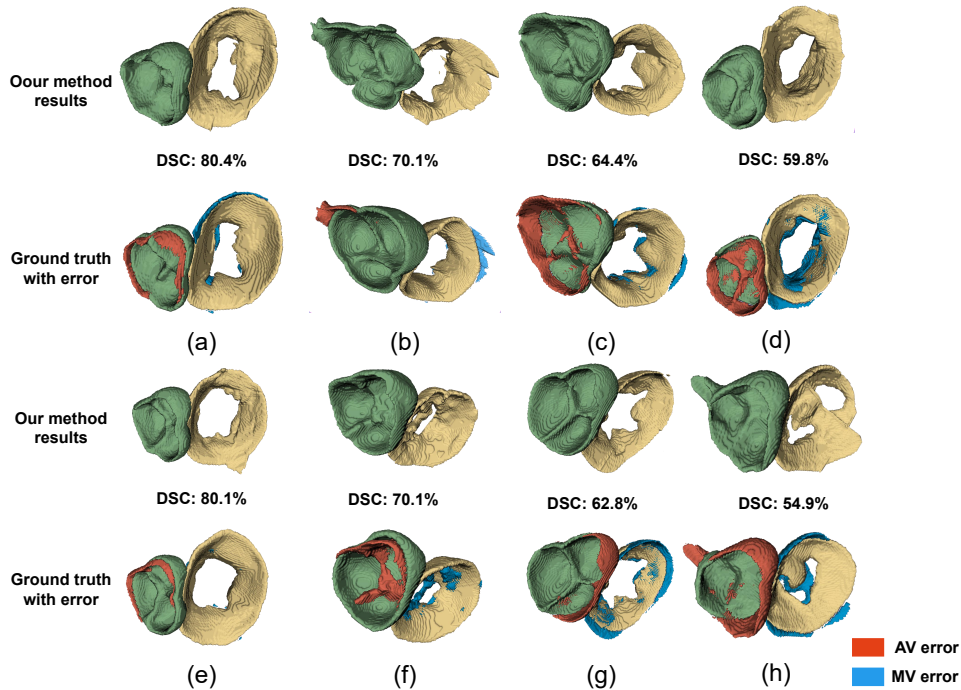
Figure 8: 3D visualization of our segmentation results with (a) and (e) best, (b-c) and (f-g) median, and (d) and (h) worst DSC among all the test images.

in Figure 8(b-c) and (g), and bad segmentation in Figure 8(h), most of the segmentation errors locate at the edges. A possible reason is that the boundary of the valve has low contrast with the surrounding tissues. In addition, the shape of valves features a thin and complex shape which also introduces difficulty in segmentation. For example, the aortic annulus is the connection of the lowest points of the valve leaflets, whereas the mitral annulus is a complex nonplanar saddle-shaped structure, which contributes to the complexity of segmentation. The segmentation error is also distributed in the inner area as shown in Figure 8(d) and (f), which is because of the difference in thickness between the segmentation and the ground truth. This is due to the fact that AV and MV are relatively small and thin membrane-like substructures in the heart. Thus, noise during the acquisition process and the imaging process can easily affect the image resulting in missing pixels of valves. These qualitative examples highlight the challenges associated with valve segmentation, including low contrast boundaries, complex valve shapes, and susceptibility to noise during image acquisition. Despite these challenges, our method demonstrates both successful segmentations and areas for potential improvement.

Qualitative illustration of the good and bad segmentation in the heart segmentation module is shown in Figure 9 and Figure 5.4. Overall, the main structures of AO, LV, LA, and myocardium are well segmented. The errors mainly come from thin structures and boundaries. For example, the thin vessels connected to the aorta (i.e., coronary vessels) as shown in Figure 9(a) are not well detected. The same error happens to LA where

thin pulmonary veins are not well detected. The boundaries of LV (Figure 5.4(c)) and myocardium (Figure 5.4(d)) are not well segmented which is due to the low contrast, making it challenging to accurately identify the boundaries. In Figure 5.4, it can be found that DSC of the excised myocardium range from 33.7% to 77.7%, which is due to the fact that excised region is largely subjective to the surgeon. Note that a rough initial segmentation can also provide the surgeon with a rough scope of the excision region thus helping the surgeon with surgical planning.
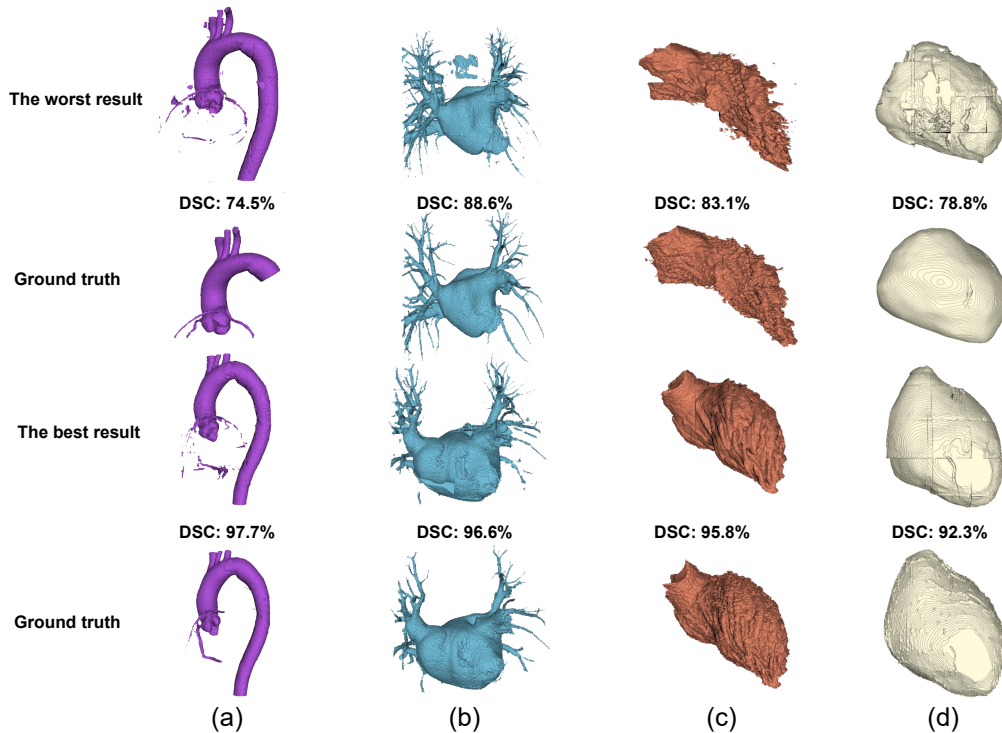

Figure 9: Visualization of (a) AO, (b) LA, (c) LV, and (d) myocardium segmentation with the best, median, and worst DSC in the heart segmentation module.

5.5. Comparison with related works

Comparison of AV and MV segmentation with related works is shown in Table 3, and the corresponding target applications and dataset size are shown in Table 4. Note that all existing methods use in-house datasets which cannot be compared fairly, and the datasets and target applications vary. In addition, the details of their code are also not easy to implement. Thus, we just list the segmentation performance in existing works here for a rough discussion. Our method obtains the optimal performance on almost all metrics except precision. Note that almost all methods achieve similar performance on precision. Considering the standard deviation, our method obtains the smallest values on all metrics compared with existing methods indicating that the proposed method is more stable. The dataset size in most existing studies is relatively small, typically consisting of around 30 samples.
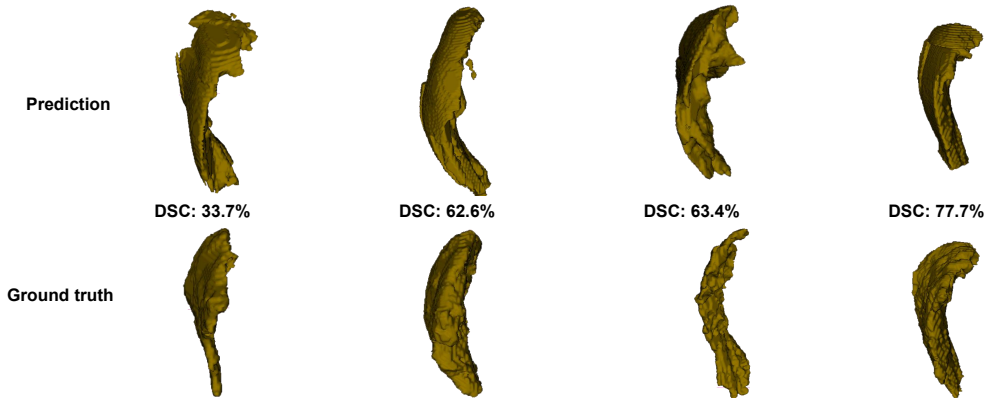
Figure 10: Visualization of the excised myocardium segmentation with the best, median, and worst DSC in the heart segmentation module.

In contrast, our dataset is comparable in scale to the existing works. This phenomenon arises primarily due to the inherent limitations in the number of surgeries conducted within clinical practice, which is significantly fewer compared to other general examinations.

Table 3: Mean and standard deviation (std) of DSC, TPR, Precision, and SO (in %) and HD95, MSD(in mm) of existing methods and our method for AV and MV segmentation. Note that all existing methods use in-house datasets which cannot be compared fairly and a rough discussion is presented here. In addition, the dataset and target applications vary for existing works and our method. Our work has published our dataset to facilitate related searches.

Method	DSC	TPR	Precision	SO	HD95	MSD
Finnegan (2020)	41.3	-	-	-	-	2.6
std	±15.9	-	-	-	-	±1.1
Jin and Hugo (2021)	39.0	-	-	-	-	8.6
std	±10.0	-	-	-	-	±3.2
Pak et al. (2020)	65.6	-	-	-	-	-
Our proposed method	**71.4**	79.5	67.0	73.8	8.0	**1.6**
std	**±8.0**	±10.5	±13.9	±9.8	±5.1	±1.0

6. Conclusion

In this paper, we integrated anatomical prior knowledge into deep learning for automatic AV and MV segmentation. Unlike general two-stage methods, we feed the refined segmentation of the left ventricle, the left atrium, and the aorta as an extra input for valves segmentation. In this way, the anatomical prior knowledge, i.e., the surrounding anatomic structures of valves, are fed into DNNs. We collected the first dataset of 27 CT images from patients with

Table 4: Target applications and dataset size of existing works and our method.

Method	Target applications	Dataset size
Finnegan (2020)	Cardiotoxic dose estimation for breast cancer patients	20 CT images
Jin and Hugo (2021)	Breast cancer radiotherapy for breast cancer patients	129 CT images
Pak et al. (2020)	Surgical planning for transcatheter aortic valve replacement	35 CT images
Our proposed method	Surgical planning for septal myectomy	27 CT images

a medical history of septal myectomy surgery. Experimental results show that our method achieves an average DSC of 71.4% and 70.0% for MV and AV, respectively, and an average improvement of 3.4% and 1.3% for MV and AV, respectively, over the existing methods. However, the segmentation is still limited for clinical practice, and there still exist cases that a major part of valves cannot be detected, and boundaries cannot be well segmented due to low contrast. Thus, we have released our dataset and code to the public Dataset.

Acknowledgments

References

Alexander Afanasyev, Alexander Bogachev-Prokophiev, Eugeniy Lenko, Ravil Sharifulin, Michael Ovcharov, Dmitriy Kozmin, and Alexander Karaskov. Myectomy with mitral valve repair versus replacement in adult patients with hypertrophic obstructive cardiomyopathy: a systematic review and meta-analysis. *Interactive CardioVascular and Thoracic Surgery*, 28(3):465–472, 2019.

Dataset. Valves segmentation hocm dataset. *https://github.com/XiaoweiXu/Automatic-Segmentation-of-Aortic-and-Mitral-Valves-for-Heart-Surgical-Planning-of-HOCM*.

Lorenzen E. Dowling J. Holloway L. Thwaites D. Brink C. Finnegan, R. Localised delineation uncertainty for iterative atlas selection in automatic cardiac segmentation. *Phys. Med. Biol.*, 65:035011, 2020. doi: 10.1088/1361-6560/ab652a.

Thomas M. A. Dise J. Kavanaugh J. Hilliard J. Zoberi I. Jin, X. and G. D. Hugo. Robustness of deep learning segmentation of cardiac substructures in noncontrast computed tomography for breast cancer radiotherapyanom. *Medical Physics*, 48:7172–7188, 2021.

Jiexu Ma, Jian Liu, Haiyun Yuan, Yajie Tang, Hailong Qiu, Jian Zhuang, and Huiming Guo. Two-port thoracoscopic myectomy for hypertrophic cardiomyopathy with three-dimensional printing. *The Annals of Thoracic Surgery*, 111(3):e165–e168, 2021.

Barry J Maron and Martin S Maron. Hypertrophic cardiomyopathy. *The Lancet*, 381(9862): 242–255, 2013.

Daniel H. Pak, Andrés Caballero, Wei Sun, and James S. Duncan. Efficient aortic valve multilabel segmentation using a spatial transformer network. In *2020 IEEE 17th International Symposium on Biomedical Imaging (ISBI)*, pages 1738–1742, 2020.

Christian Payer, Darko Štern, Horst Bischof, and Martin Urschler. Multi-label whole heart segmentation using cnns and anatomical label configurations. In *International Workshop on Statistical Atlases and Computational Models of the Heart*, pages 190–198. Springer, 2017.

Tom Wang Chengjia, MacGillivray, Gillian Macnaught, Guang Yang, and David Newby. A two-stage 3d unet framework for multi-class segmentation on full resolution image. *arXiv preprint arXiv:1804.04341*, 2018. URL https://arxiv.org/abs/1804.04341.

Xiaowei Xu, Qing Lu, Lin Yang, Sharon Hu, Danny Chen, Yu Hu, and Yiyu Shi. Quantization of fully convolutional networks for accurate biomedical image segmentation. In *CVPR*, pages 8300–8308, 2018.

Xiaowei Xu, Tianchen Wang, Yiyu Shi, Haiyun Yuan, Qianjun Jia, Meiping Huang, and Jian Zhuang. Whole heart and great vessel segmentation in congenital heart disease using deep neural networks and graph matching. In *MICCAI*, pages 477–485, 2019.

Xiaowei Xu, Tianchen Wang, Jian Zhuang, Haiyun Yuan, Meiping Huang, Jianzheng Cen, Qianjun Jia, Yuhao Dong, and Yiyu Shi. Imagechd: A 3d computed tomography image dataset for classification of congenital heart disease. In *MICCAI*, pages 77–87, 2020.

Xiaowei Xu, Qianjun Jia, Haiyun Yuan, Hailong Qiu, Yuhao Dong, Wen Xie, Zeyang Yao, Jiawei Zhang, Zhiqaing Nie, Xiaomeng Li, et al. A clinically applicable ai system for diagnosis of congenital heart diseases based on computed tomography images. *Medical Image Analysis*, page 102953, 2023.

Xin Yang, Cheng Bian, Lequan Yu, Dong Ni, and Pheng-Ann Heng. Hybrid loss guided convolutional networks for whole heart parsing. In *International workshop on statistical atlases and computational models of the heart*, pages 215–223. Springer, 2017.

Xiahai Zhuang and Juan Shen. Multi-scale patch and multi-modality atlases for whole heart segmentation of mri. *Medical image analysis*, 31:77–87, 2016.

Xiahai Zhuang, Lei Li, Christian Payer, Darko Štern, Martin Urschler, Mattias P Heinrich, Julien Oster, Chunliang Wang, Örjan Smedby, Cheng Bian, et al. Evaluation of algorithms for multi-modality whole heart segmentation: an open-access grand challenge. *Medical image analysis*, 58:101537, 2019.